Available online at website: https://journal.bcrec.id/index.php/bcrec

Bulletin of Chemical Reaction Engineering & Catalysis, 20 (1) 2025, 20-34

Research Article

Biosynthesis of Gold Nanoparticles using Amomum subulatum and Their Catalytic Properties

Sonam Baghel, Monika Khurana*

School of Engineering & Technology, Sushant University, Sector-55, Gurugram-122003-Haryana, India.

Received: 15th October 2024; Revised: 27th December 2024; Accepted: 28th December 2024
Available online: 31th December 2024; Published regularly: April 2025

Abstract

Recent studies reveal that gold nanoparticles possess unique and promising applications, such as targeted drug delivery, cancer therapy, and environmental uses like water purification and pollutant detection. Thus, developing AuNPs through simple, eco-friendly, and cost-effective methods is crucial compared to traditional chemical synthesis. In this study, we employed a one-step method to prepare gold nanoparticles using seed extract from black cardamom. The nanoparticles were synthesized by mixing the seed extract and gold(III) chloride trihydrate in an aqueous solution on a magnetic stirrer at room temperature, with the seed extract acting as both a reducing and capping agent. The resulting wine-red colloidal AuNPs were characterized by UV-visible spectroscopy, showing a surface plasmon resonance band at 530.5 nm, indicating successful formation and stability of the nanoparticles over 2 months. the AuNPs had sizes ranging from 20 to 60 nm as revealed by transmission electron microscopy (TEM) and dynamic light scattering (DLS) studies and were predominantly spherical in shape with few being triangular. Fourier transform infrared spectroscopy (FTIR) detected the presence of functional groups on the biosynthesized AuNPs before and after reduction. A time-dependent comparative analysis of their catalytic activity demonstrated their effectiveness in degrading 4-nitro phenol and organic dyes like methylene blue, and methyl orange, achieving a degradation efficiency of 91%. Kinetic studies indicated that the reaction followed pseudo first-order kinetics.

Keywords: Gold nanoparticles; Catalytic activity; Green Synthesis; Black cardamom; p-nitrophenol

How to Cite: Baghel, S., Khurana, M. (2025). Biosynthesis of Gold Nanoparticles using Amomum subulatum and Their Catalytic Properties. *Bulletin of Chemical Reaction Engineering & Catalysis*, 20 (1), 20-34. (doi: 10.9767/bcrec.20229)

Permalink/DOI: https://doi.org/10.9767/bcrec.20229

1. Introduction

Nanoparticles are at the forefront of technological innovation, offering transformative solutions across various fields [1]. These nanoscale structures vary from 1 nanometer to 100 nanometers and characterized by differing particle size, shape, and distribution [2]. There is growing interest in gold nanoparticles (AuNPs) among the existing nanomaterials since gold is an inert material that is resistant to oxidation, making its use in nanoscale technologies and devices particularly attractive [3]. These nanoparticles are widely used in nanotherapeutics that can address several of the problems with conventional drug delivery, including those related to drug solubility, targeting, biodistribution , bioavailability, and therapeutic index [4]. Due to the presence of multifunctional theranostic facilities, nanoparticles based on metals or metal oxides such as gold, copper, titanium, zinc, etc., have promising outcomes for various biomedical applications [5]. There is a noticeable difference between the properties of bulk nanoparticles and those of synthesized nanoparticles. The preparation of metal nanoparticles can be conducted in a number of physical, chemical, and

* Corresponding Author.
Email: monikakhurana@sushantuniversity.edu.in (M. Khurana)

biological ways, utilizing metals such as gold, zinc, copper, palladium, and so forth. Physical and chemical methods have many disadvantages and pose harmful effect on the environment, therefore biological methods are preferred. These biological method employs plant parts or microorganisms, such as fungi, bacteria, etc., to synthesize nanoparticles. Some plants exhibit functional compounds which includes phenols, alkaloids, saponins, polysaccharides, proteins, and organic acids [6]. Aside from being environmentally friendly and cost-effective, they are also easy to scale up for large scale synthesis and don't require high pressure, high energy, high temperature or toxic chemicals. It may be more efficient and cost effective to synthesize nanoparticles from plant extracts than through other biological methods since it requires no elaborate preservation of cell cultures, is suitable for large scale synthesis and more affordable [7]. There are various phytoconstituents in them that act as stabilizing and reducing agents in the production of nanoparticles. There is no need of adding any other reducing or stabilizing agent. Medicinal plants are a natural source to prepare nanoparticles through green synthesis and they act as antimicrobics, antioxidants, anticancers[8], etc. Green synthesis of nanoparticles from these plants is all the more exciting because nanoparticles are smaller, have a huge surface area, and have more potential. This green synthesis method is rapid, simple, easy, and ecofriendly[9]. Gold nanoparticles (AuNPs) have fascinated scientists and technologists over the years because of their catalytic, magnetic, optical, chemical properties, and possess electrical conductivity, and surface enhanced Raman scattering (SERS) [10].

It is widely recognized that gold nanoparticles have a unique and tunable surface Plasmon resonance (SPR) and are used in biomedical science in a variety of ways, including drug delivery, tissue/tumor imaging [11], photothermal therapy [11], and identification of pathogens using immunochromatography [12,13]. The unique properties of AuNPs make them an ideal choice for use in biomedicine, biosensors, and electronic devices [14]. As a result of their small particle size and high loading capacity, they promote the solubility of the herbal medication and concentrate the drug in a specific area of the body, resulting in greater efficacy. Because of these distinctive properties, metal nanoparticles are used in a range of biomedical applications, including cancer therapies [11], antibacterial agents, and gene transplantation [11]. Nanoparticles synthesized for medical purposes must be biocompatible and either low- or non-toxic. Nanoparticles made of metals, such as platinum, palladium, silver, and gold, have been extensively tested on humans. They are less toxic to animal and microorganism cells than other metal nanoparticles. Since gold metal is considered to be the most recognized metal nanoparticle for health applications due to its biocompatibility and surface modifiability, therefore, we chose gold metal as our material of choice [15]. Gold nanoparticles (AuNPs) can be synthesized in a variety of sizes and shapes such as triangular [16], hexagonal, spherical, and irregular shapes [17].

This study explored the potential of utilizing black cardamom extract for the green synthesis of AuNPs. Exploring the use of black cardamom extract for nanoparticle synthesis offers a novel approach and contributes to the growing body of research on green nanotechnology. The presence of various bioactive compounds in black cardamom extract may influence the size, shape, and surface properties of the synthesized nanoparticles, potentially leading to unique and desirable characteristics for specific applications. The dried fruit of Black Cardomom (BC) is the fruit of a perennial herbaceous plant in the family Zingiberaceae [5]. This is one of the most important commercial crops in the Eastern Himalayan Region. It is grown in marshy areas near streams, across hills. Spices such as this one are well-known for their distinct taste and aroma, and are commonly used to enhance dishes from the Himalayan area, which includes Nepal, Bhutan, and India. BC is extensively used in ethnomedicine according to Ayurvedic and Unani medical systems. This herb is traditionally used to treat coughs, lung congestion, pain, stomach disorders, and a variety of other ailments. The advent of modern phyto-analytical and pharmacological techniques as well as the recent popularity of natural products-based medicine have resulted in new therapeutic applications of this ancient spice. There have been recent studies indicating that BC contains high levels of polyphenols, which may help to reduce and stabilize nanoparticles [18]. As a result of their bioactive properties, these compounds possess antioxidant [19], antimicrobial [20], antibacterial [21] antifungal, analgesic, anti-inflammatory [22], anticancer [23], cardio-adaptogen [24], and hypolipidemic properties. In the process of forming nanoparticles, the polyphenolic compounds present in amomum subalatum seed extract act both as a reducing and stabilizing agent. In addition, the waste peels of BC are also used in the removal of Cd(II) from water [25] and congo red from water [26].

Our study provides a new, ecocompatible, and green way of synthesizing AuNPs from Au(II) salts using seed extract of BC as a natural reducer without any additional additives to prevent aggregation of nanoparticles [27]. Green synthesis

of AuNPs utilizing black cardamom extract offers significant environmental advantages. By employing a non-toxic, plant-based reducing agent derived from a renewable resource, this eco-friendly approach eliminates the need for hazardous chemicals typically used in conventional AuNP synthesis. The process is conducted under mild conditions, such as room temperature in aqueous media, minimizing energy consumption and avoiding the use of organic solvents. Furthermore, this method demonstrates rapid synthesis capabilities and allows for control over the size and shape of the resulting AuNPs by adjusting reaction parameters. This green synthesis strategy aligns with the principles of sustainable chemistry, providing a more environmentally responsible and potentially more efficient alternative to traditional AuNP production methods.

2. Material and Methods

2.1 Materials

Tetra chloroauric(III) acid trihydrate or Chloroauric acid ($HAuCl_4.3H_20$), Sodium Borohydride ($NaBH_4$), p-nitrophenol, Methylene Blue (MB) and Methyl orange (MO) were purchased from Sigma Aldrich. Analytical grade chemicals and reagents were used throughout the study. In all experiments, MilliQ water of resistivity 18.2 MΩ·cm at 25 °C was used. The seed pods of *Amomum subulatum* (commonly called black cardamom, BC) were bought from a local market. A plant authenticity study on black cardamom was conducted at CSIR-NIScPR, New Delhi, India.

2.2 Preparation of Seed Extract and Biosynthesis of AuNPs

Seed extract was prepared using BC seeds. BC seeds were washed twice in double distilled water to remove foreign particles, dried out in an oven at 50 ^{0}C for 30 minutes, and then ground into a fine powder using a pestle and mortar. 5 g of freshly prepared dry seed powder was dissolved in 100ml of distilled water [28] and boiled for 1 hour 30 minutes at 75 ^{0}C on magnetic stirrer [29]. Filtering the prepared seed extract was performed using Whatman filter paper no. 1. The supernatant was kept at 4 °C for further experimental use. 1 mM Gold(III) chloride trihydrate was prepared in MiliQ water. It was heated at room temperature and then seed extract was added to it. The ratio of gold chloride solution and seed extract was kept at 1:1 (v/v) and 1:0.5 (v/v). It was kept on magnetic stirrer until the color changed from yellow to wine red which indicated the synthesis of 1:1 ratio AuNPs and 1:0.5 ratio AuNPs [30]. The Studies confirmed that synthesized AuNPs are stabilized over a period of 12 weeks. The possible mechanism involved in the synthesis of AuNPs has been depicted in Figure 1.

The possible Simple reaction process is shown below:

Dissociation of Gold salt:

$$HAuCl_4 \rightleftharpoons H^{\oplus} + Au^{3+} + 4Cl^{\ominus} \quad (1)$$

Oxidation Process:

$$4Cl^{\ominus} \rightleftharpoons 2Cl_2 + 4e^- \quad (2)$$

Reduction process:

$$Au^{3+} + 4e^- \rightleftharpoons Au^0 + e^- \quad (3)$$

2.3 Characterization of Green Synthesized AuNPs

UV – Vis Spectroscopy – The stability of AuNPs was assessed using UV-Vis spectrophotometry (Shimadzu UV-1800). Milli Q water served as the blank. Absorbance measurements were recorded from 300 nm to 700 nm. For spectral analysis, 1 mL of the prepared colloidal AuNPs solution was added to a cuvette and diluted with 2 mL of MilliQ water.

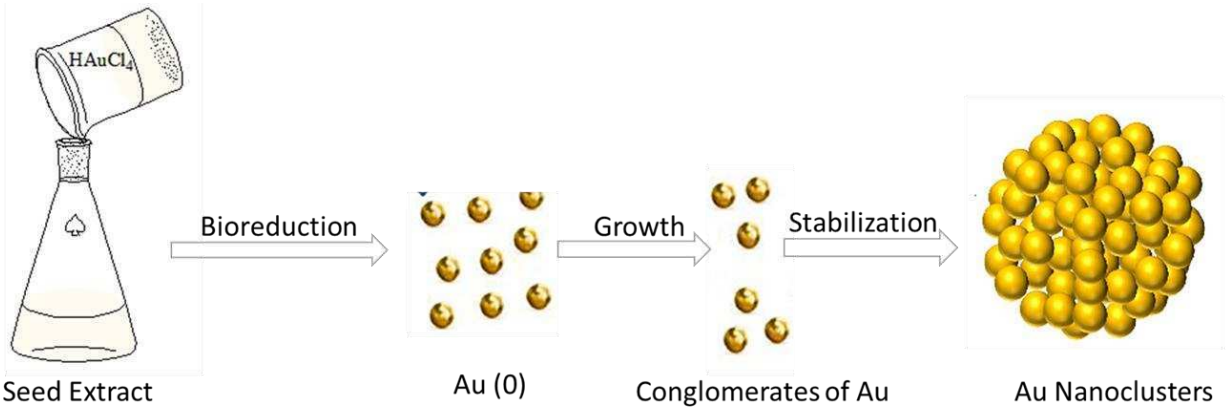

Figure 1. Hypothetical mechanism of AuNPs formation

TEM Analysis of Gold Nanoparticles – To characterize the morphology, size distribution, and aggregation of the AuNPs, high-resolution transmission electron microscopy (TEM) was performed using a TALOS 200 KV microscope. Prior to TEM grid preparation, the synthesized AuNP colloidal solution was centrifuged at 10,000 rpm for 15 minutes at 25 °C. The supernatant was collected and used for subsequent TEM analysis. To ensure proper dispersion, the AuNP-containing supernatant was sonicated before pipetting 10 µL onto a carbon-coated TEM grid. The grid was then air-dried. Nanoparticle size was determined by analyzing images captured at various magnifications.

FTIR – for FTIR measurements, FTIR spectrophotometer Shimadzu IR affinity 1S was used to collect infrared spectra of the BC extract before and after reduction of AuNPs to characterize the AuNPs surfaces. FTIR is used to find and classify probable biomolecules that can cap, thereby stabilizing AuNPs efficiently [31]. According to literature investigation, a comprehensive analysis of Black Cardamom (BC) revealed a complex chemical profile comprising 40 distinct compounds. Notably, 1,8-cineole emerged as the predominant component, constituting approximately 65% of the total composition. Pinene and terpineol were identified as other key constituents, accounting for 0.85% and 7.92%, respectively [32]. 30 µL of AuNps solution was spreaded on the sample cell and spectra was recorded. FTIR spectra were subsequently recorded for both the plant extract and the synthesized AuNPs.

DLS –Zeta potential and hydrodynamic size of the AuNPs were measured using a Zetasizer Nano ZS (Malvern Instruments Ltd.). Prior to DLS analysis, the AuNP solution was centrifuged at 10,000 rpm for 10 minutes, and the supernatant was collected. 1 mL of the centrifuged supernatant was then used for DLS measurements. Zeta potential provides valuable information regarding the dispersion stability of nanoparticles in solution. The stability of the dispersion is strongly influenced by the zeta potential, which is in turn affected by factors such as pH and electrolyte concentration. Studies indicate that a zeta potential exceeding +30 mV or below -30 mV generally signifies a stable dispersion [33].

2.4 Application of AuNPs: Catalytic Efficiency of Gold Nanoparticles

2.4.1 Conversion of p-nitrophenol into p-aminophenol

Industrial waste, particularly from dye and agrochemical manufacturing, significantly contributes to water pollution. p-Nitrophenol, a highly stable and harmful compound, is released during these processes. However, it can be readily transformed into p-aminophenol, a safe compound with valuable applications in pharmaceutical synthesis. AuNPs exhibit catalytic activity due to their high surface-to-volume ratio and numerous surface-active sites. The conversion of p-nitrophenol into p-aminophenol was monitored using UV-Vis spectrophotometry, with spectra recorded in triplicate. To assess catalytic activity, 80 µL of freshly prepared 3×10^{-1} M $NaBH_4$ solution was added to 2 mL of 1×10^{-4} M p-nitrophenol solution. The immediate color change was observed and quantified using UV-Vis spectroscopy. Subsequently, varying volumes (50 µL, 100 µL, and 200 µL) of the AuNPs colloidal solution (catalyst) were added, and the reaction progress was monitored at room temperature and atmospheric pressure. UV-Vis spectra were recorded at 2-minute intervals from 200 to 600 nm, and the resulting data was plotted as absorbance versus wavelength using Origin Pro software [34].

2.4.2 Reduction/degradation of organic dyes

Organic dyes are a major source of water pollution, with detrimental consequences for human health. Methylene Blue (MB), a thiazine dye with the chemical structure 3,7-bis(dimethylamino)-phenothiazin-5-iumchloride, has diverse applications. These include the detection of sulfide ions in aquatic environments, its use as a chemotherapeutic and antimicrobial agent in aquaculture [35], and its utilization in surgical, microbiological, and diagnostic procedures [36]. Organic dyes discharged into aquatic environments pose a significant threat to both the environment and human health. These dyes, primarily from the textile, dyeing, and printing industries, not only cause aesthetic issues but also have detrimental effects on aquatic life. Furthermore, the consumption of water contaminated with these dyes can have adverse impacts on human health.

2.4.3 Degradation of Methylene blue (MB)

To study degradation of MB, 1 mM solutions of MB was prepared in Milli Q water. To study dye degradation, 1 mL of MB was mixed with 1 mL of 100 mM $NaBH_4$ solution and total volume is made up to 12 mL and 2 mL of AuNPs (catalyst) was added. The dye degradation was monitored by measuring absorbance from 200 to 800 nm at room temperature, atmospheric pressure using UV-Vis spectrophotometer at 2 min time intervals and graphs were plotted between absorbance and wavelength using origin pro. Control experiment was also performed using a mixture of dye solution and additionally, $NaBH_4$ was performed

for the purpose of providing comparison [37]. Experiments were performed in triplicates.

2.4.4 Degradation of Methyl Orange (MO)

To investigate the degradation of Methyl Orange (MO), a 10 mg/L solution of MO was prepared using Milli-Q water. For dye degradation studies, MO was mixed with 2 mL of 0.2 M $NaBH_4$ solution and 1 mL of AuNP colloidal solution (catalyst). The degradation of the dye was monitored by recording UV-Vis absorbance spectra from 200 to 800 nm at 2-minute intervals under ambient conditions (room temperature and atmospheric pressure). Absorbance values were plotted against wavelength using Origin software. A control experiment was also performed using a mixture of the dye solution and $NaBH_4$ to provide a comparative baseline. All experiments were conducted in triplicate.

3. Result and Discussion

3.1 Characterisation of AuNPs

3.1.1 UV spectroscopy

UV-visible spectroscopy is a crucial technique for characterizing metal nanoparticles, providing information on their stability and synthesis. The observed absorption bands in nanoparticle solutions are a result of surface plasmon resonance, which involves the collective oscillations of electrons within the metal nanoparticles. By analyzing these spectral features, valuable information regarding nanoparticle size and shape can be obtained [38]. To characterize the synthesized AuNPs, UV-Vis spectroscopy was performed immediately. 1 mL of the reaction mixture was diluted with 3 mL of double-distilled water for spectral analysis. Figure 2 displays the recorded spectrum. The observed absorption maximum at 530.5 nm confirms the formation of AuNPs. The absence of any significant peaks between 450 and 700 nm indicates the absence of AuNP aggregation.

Previous research has demonstrated that the properties of metal nanoparticles are closely linked to their surface plasmon resonance peak position and intensity [39]. The seed extract of BC is rich in phytochemicals, including flavonoids and phenolic compounds. During AuNP synthesis, these phytochemicals act as both reducing and stabilizing agents. In this study, a solution containing $HAuCl_4.3H_2O$ was mixed with the seed extract, leading to the reduction of Au^{+3} ions to Au atoms, which subsequently aggregated to form nanoparticles. Furthermore, the phytochemicals effectively stabilized the synthesized AuNPs by forming a protective coating, preventing their aggregation. Figure 2(b) presents the UV spectra of the synthesized AuNPs at 1:1 and 1:0.5 ratios. As shown in Figure 2(c), the surface plasmon resonance (SPR) band of the AuNPs remained remarkably stable even after several months of storage at ambient temperature, further confirming the efficacy of the phytochemicals in stabilizing the nanoparticles [38].

3.1.2 TEM analysis

Transmission electron microscopy (TEM) was employed to characterize the synthesized AuNPs, revealing their morphology and size distribution. Figure 3(a) demonstrates that all

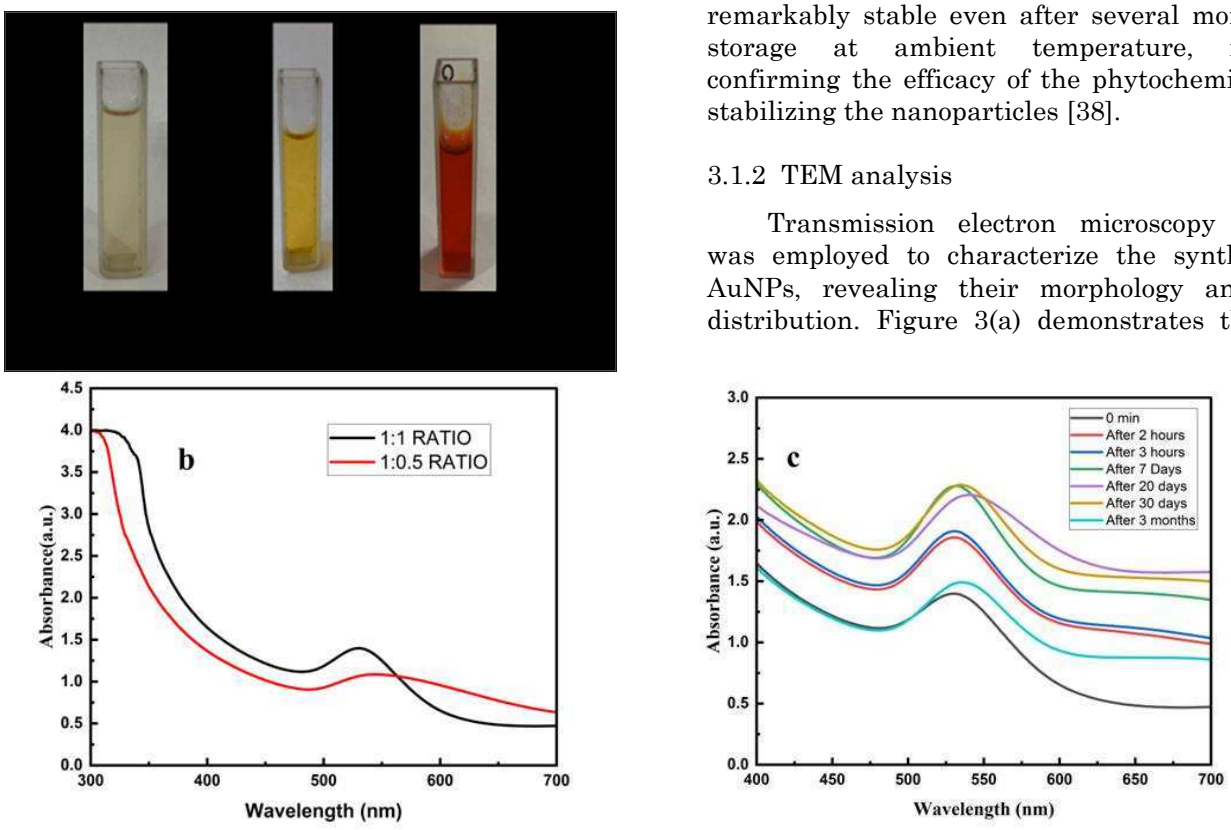

Figure 2. (a) Images of Plant Extract, Gold Nitrate solutions and Colloidal Solution of synthesized AuNPs (b) UV-Visible absorption spectra of synthesized gold nanoparticles stabilized in BC (c) Time variation from 0 to 3 months

AuNPs observed were less than 100 nm in size. A magnified view of this morphology is presented in Figure 3(b), showcasing a mixture of triangular and spherical AuNPs, along with some capping agents, at a resolution of 10 nm. In contrast to the 1:1 ratio shown in Figure 3, AuNPs synthesized at a 1:0.5 ratio (Figure 4) exhibited a broader range of shapes, observed at varying resolutions. Overall, the synthesized particles were predominantly spherical, with a proportion exhibiting triangular morphologies.

3.1.3 FTIR analysis

FTIR spectroscopy was employed to investigate the role of BC extract in AuNP formation. The recorded FTIR spectra of the BC extract provided valuable information regarding the functional groups of the chemical compounds present within the extract. FTIR spectra were acquired from 30 µL of BC extract both before and after the bioreduction of gold nanoparticles. A comparison of these spectra revealed shifts in certain peak positions within the 4000-3200 cm^{-1} range, indicating potential interactions between the phytochemicals in the extract and the synthesized AuNPs. There is a broad peak around 3259 cm^{-1} which attributes O–H stretching vibrations of various phenolic compounds. The peak at 2959 cm^{-1} is characteristic of aliphatic C–H stretching vibrations. The moderately strong band at 1637 cm^{-1} could be assigned to C=C stretching vibrations of aromatic ring. The peaks at 1031 cm^{-1} corresponds to C–O stretching vibrations of phenolic groups. Other bands up to

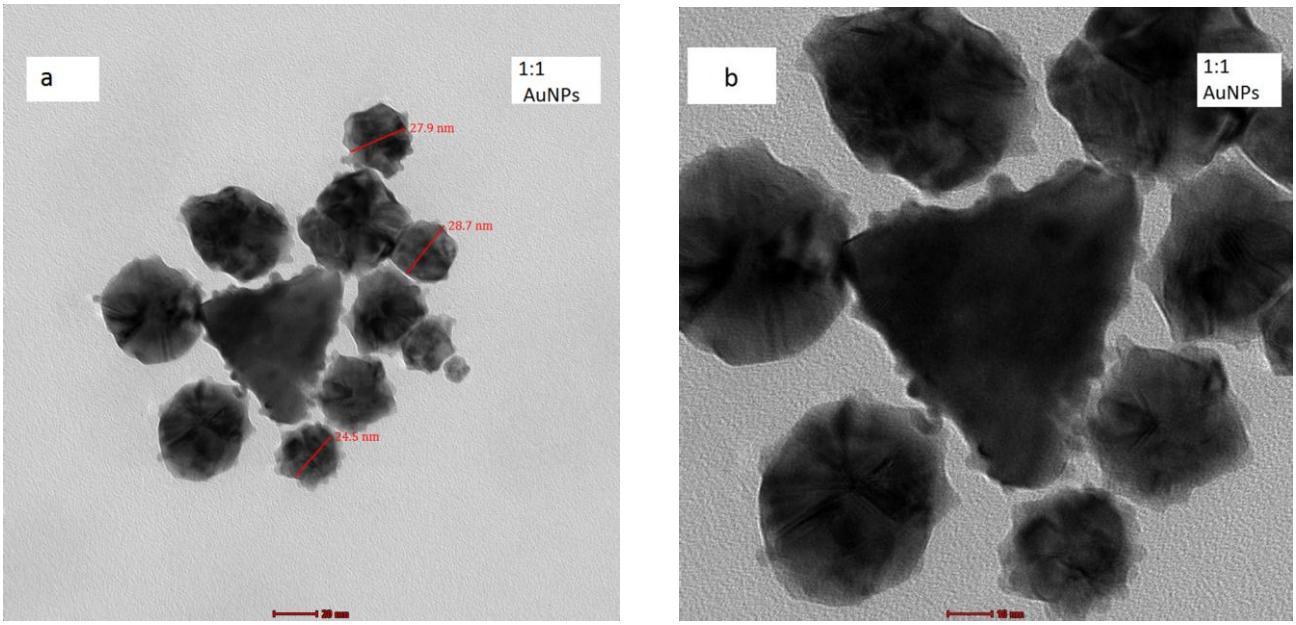

Figure 3. HR-TEM images of 1:1 synthesized Gold nanoparticle under different magnification (a) at 20 nm showing different sizes (b) at 10 nm.

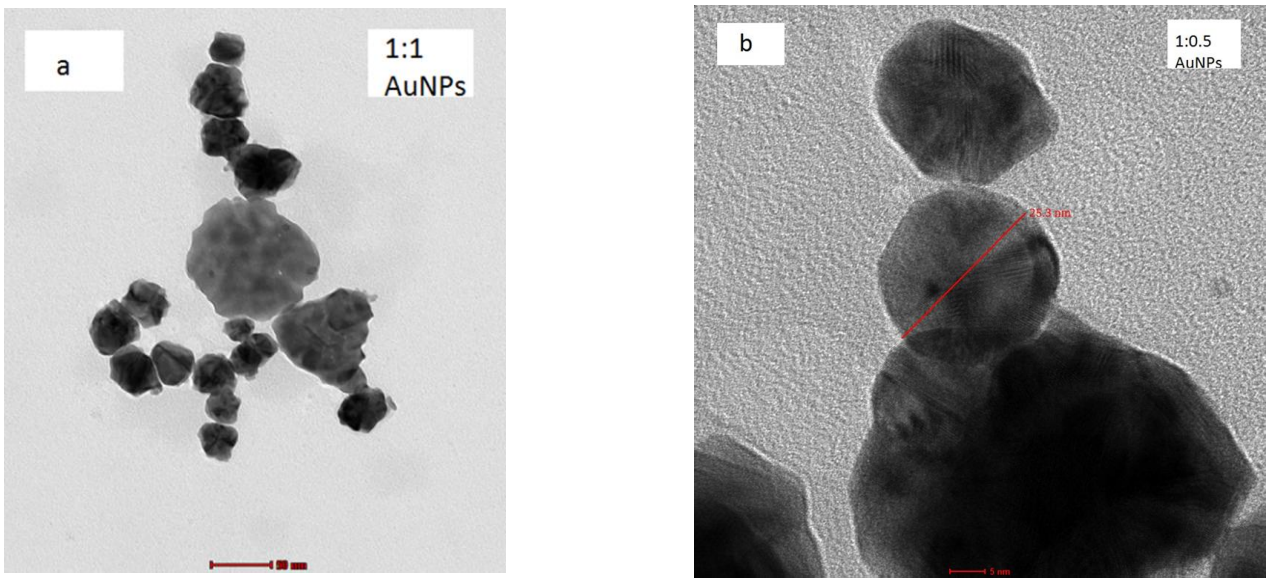

Figure 4. HR-TEM images of 1:0.5 synthesized gold nanoparticles under different magnification (a) at 50 nm (b) at 5 nm.

1800 cm^{-1} are also found in both spectra, that is, in both spectra obtained before and after the reduction. After 1770 to 500 cm^{-1}, the positions of bonds are again almost similar as those before reduction, with varying intensity as presented in Table 1.

Figure 5 shows that certain peaks in the FTIR spectra remained consistent before and after the bioreduction of the plant extract, while minor shifts were observed in the peaks associated with phenolic compounds and the C=C stretching of aromatic rings. These functional groups likely played a crucial role in the bioreduction of Au^{+} ions. They may have acted as robust binding sites and electron-rich centers, facilitating the conversion of gold ions into AuNPs. These findings align with previous studies that have demonstrated the involvement of biomolecules in the reduction of Au ions during the formation of AuNPs.

3.1.4 DLS measurements

DLS analysis was performed to determine the zeta potential and average hydrodynamic diameter of the synthesized AuNPs. DLS measurements revealed a size distribution for the AuNP colloidal solution ranging from 12 nm to 60 nm, with a Z-average of 113.1 nm. It is important to note that DLS measurements typically yield slightly larger size values compared to those obtained from TEM analysis [40]. The resulting size depends on the size of the AuNPs metal core, the biomaterial absorbed onto their surface, and electric double layer (solvent wall) that flows between particles [41,42]. The poly dispersive index (PDI) of the measurements represents the size distribution within a sample [43]. The synthesized AuNPs exhibited a narrow size distribution, as evidenced by PDI values of 0.301 for the 1:1 ratio (Figure 6(a)) and 0.289 for the 1:0.5 ratio (Figure 7(a)). A PDI value below 0.5 generally indicates a relatively narrow particle size distribution, while values closer to zero suggest a more uniform, monodisperse sample. Zeta potential measurements revealed a negative surface charge for the synthesized AuNPs, with values of -10.3 mV for the 1:1 ratio (Figure 6(b)) and -7.58 mV for the 1:0.5 ratio (Figure 7(b)). This negative surface charge contributes to the stability of the colloidal dispersion by minimizing particle aggregation.

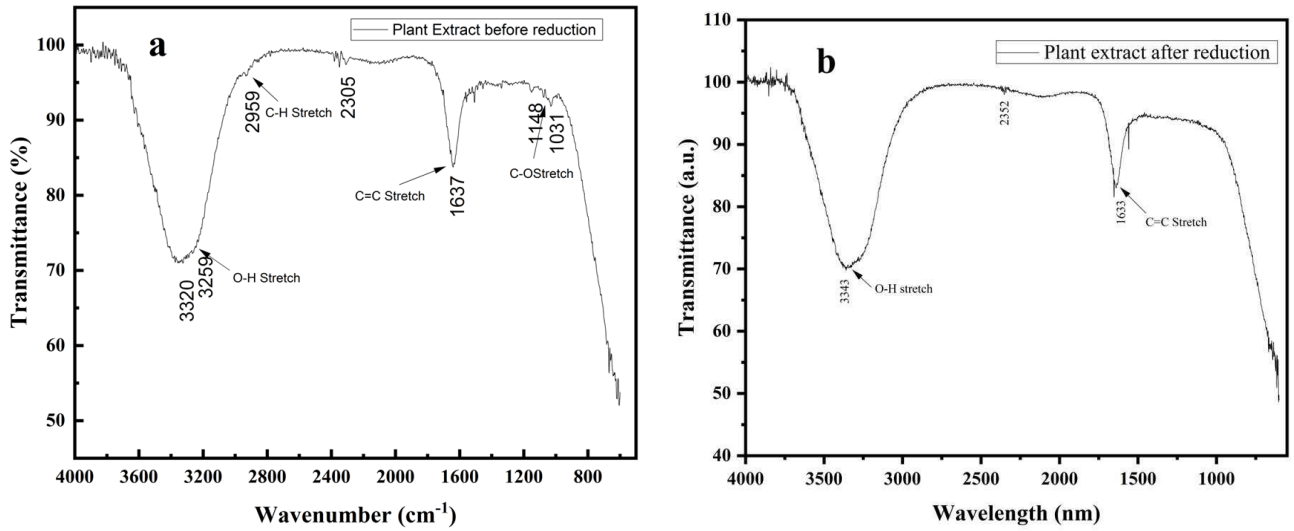

Figure 5. FT-IR spectra of plant extract (a) before reduction and (b) after reduction of plant extract

Table 1. FTIR spectra of plant extract before and after reduction representing the wavenumbers of the various functional groups.

Functional groups	Wavenumbers
O–H streching vibrations of phenolic compounds	3259 cm^{-1}
aliphatic C–H stretching vibrations	2959 cm^{-1}
C=C stretching vibrations of aromatic ring	1637 cm^{-1}
C–O stretching vibrations of phenolic groups	1031cm^{-1}
Other bands (both spectra obtained before and after the reduction)	1800 cm^{-1}
(both spectra obtained before and after the reduction)	After 1770 to 500 cm^{-1}

3.1.5 Energy Dispersive X-Ray analysis (EDX)

Energy-dispersive X-ray spectroscopy (EDS) is a powerful technique for determining the elemental composition of extremely small samples, even those as minute as a few cubic micrometers. In a scanning electron microscope (SEM), the focused electron beam interacts with the sample's surface, exciting the atoms and causing them to emit characteristic X-rays. These X-rays, unique to each element, are then detected and analyzed by an energy-dispersive detector. By analyzing the energies of these X-rays, the elemental composition of the sample's surface can be precisely determined [44].

EDX analysis of the synthesized AuNPs revealed strong signals characteristic of gold, confirming the presence of AuNPs. The detection of elements such as Mg, Cl, K, and Ca can be attributed to the adsorption of organic moieties from the BC seed extract onto the AuNP surface. These organic compounds, which act as reducing and stabilizing agents during AuNP synthesis, may contribute to the presence of these elements. AuNPs synthesized using the aqueous extract of BC exhibited a broad energy-dispersive X-ray absorption spectrum. Weak signals corresponding to K, C, Cu, Ca, and Cl were observed. Further chemical examination, as depicted in Figure 8, confirmed the presence of these elements (Cl, Ca,

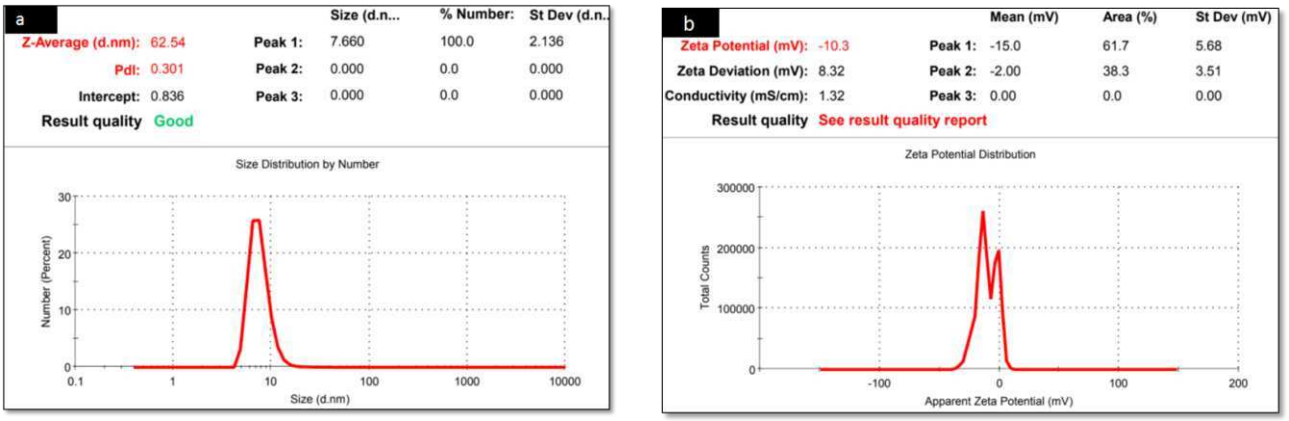

Figure 6. (a) size distribution and (b) Zeta potential of 1:1 ratio AuNPs.

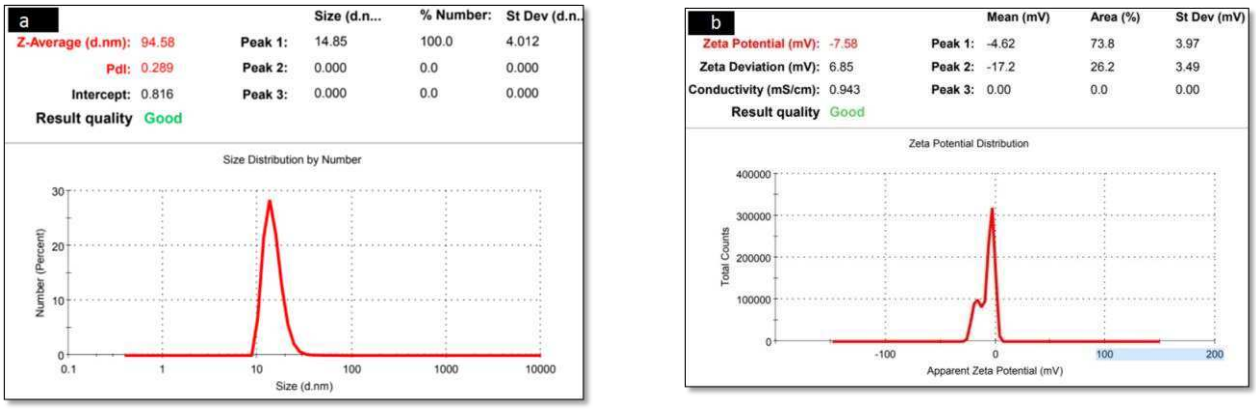

Figure 7. (a) size distribution and (b) Zeta potential of 1:0.5 ratio AuNPs

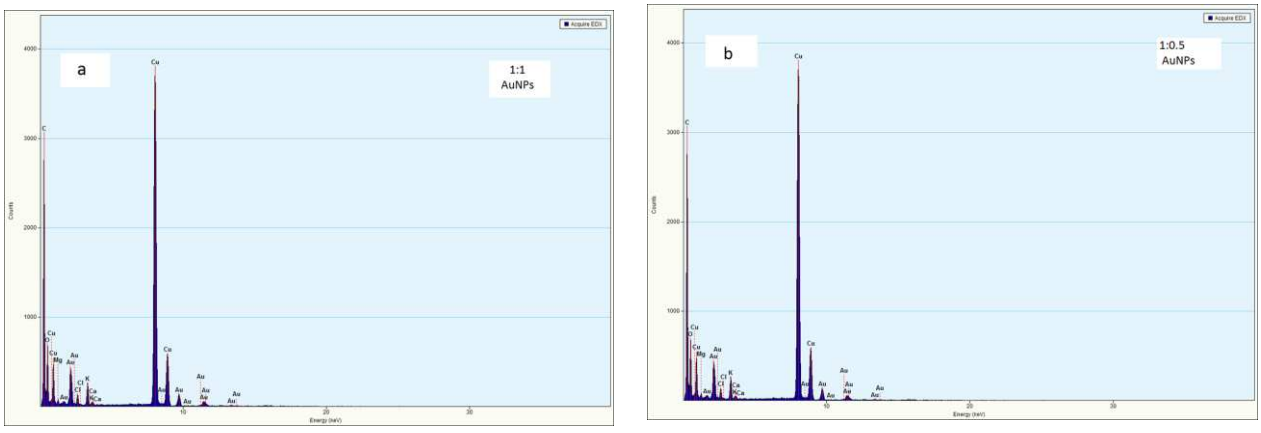

Figure 8. DX of (a) 1:1 ratio and (b) 1:0.5 ratio of synthesized AuNPs

O, Mg, K, and Au) within the synthesized nanoparticles.

3.1.6 Diffraction of AuNPs

The selected-area electron diffraction (SAED) pattern in Figure 9 provides evidence of the crystalline nature of the nanoparticles. The presence of distinct diffraction spots corresponding to the (111), (200), (220), and (311) crystal planes confirm the crystalline structure of the synthesized nanoparticles. The diffraction rings also suggested that the NPs were polycrystalline [45].

3.2 Applications of AuNPs: Catalytic Activity of AuNPs

3.2.1 Reduction of p-nitrophenol (4-NP)

The synthesized AuNPs demonstrated high catalytic activity in the reduction of p nitrophenol (4-NP) to p-aminophenol (4-AP). Degradation efficiencies of 93.67%, 66.07%, and 97.07% were achieved using 50 µL, 100 µL, and 200 µL of the AuNP colloidal solution, respectively. Kinetic analysis revealed that the reaction follows pseudo-first-order kinetics with rate constants of 0.093, 0.18, and 0.45 min^{-1} for the respective AuNP concentrations.

To prevent photocatalytic reduction of 4-NP, all experiments were conducted under dark conditions. The reduction of 4-NP by $NaBH_4$ was monitored using UV-Vis spectroscopy. Upon addition of $NaBH_4$ to the 4-NP solution, the color changed to yellow due to the formation of sodium p-nitrophenolate, with a characteristic absorption peak at 400 nm. Upon subsequent addition of AuNPs, a rapid decrease in the absorbance at 400 nm was observed, accompanied by a concurrent increase in absorbance at 300 nm, indicating the formation of 4-AP. This catalytic reduction was completed within 10 minutes, 6 minutes, and 7 minutes for 50 µL, 100 µL, and 200 µL of AuNPs, respectively.

The high catalytic activity of AuNPs can be attributed to their ability to lower the activation energy of the reaction. The absorbance of 4-NP is directly proportional to its concentration, where A_0 represents the initial absorbance and A_t represents the absorbance at time 't'. Degradation efficiency was calculated using the following formula:

$$Degradation\ Efficiency\ (\%) = \frac{(A_0 - A_t)}{A_0} \times 100\% \quad (1)$$

Due to the significantly higher concentration of $NaBH_4$ compared to 4-NP, the reaction can be approximated as pseudo-first-order kinetics. Under these conditions, the rate of the reaction is independent of the $NaBH_4$ concentration.

The rate constant (k) of the reaction was determined using the following equation:

$$k = \ln\left(\frac{A_0}{A_t}\right)/time \quad (2)$$

Figures 10(b), 11(b), and 12(b) illustrate the linear relationship between ln (A_0/A_t) and *time*, confirming the pseudo-first-order kinetics of the reaction.

Present study demonstrates a significantly reduced degradation time compared to previous work. While a previous study reported a degradation time of 13 minutes, our method achieved degradation within 6 minutes, indicating a substantial improvement in reaction kinetics [34].

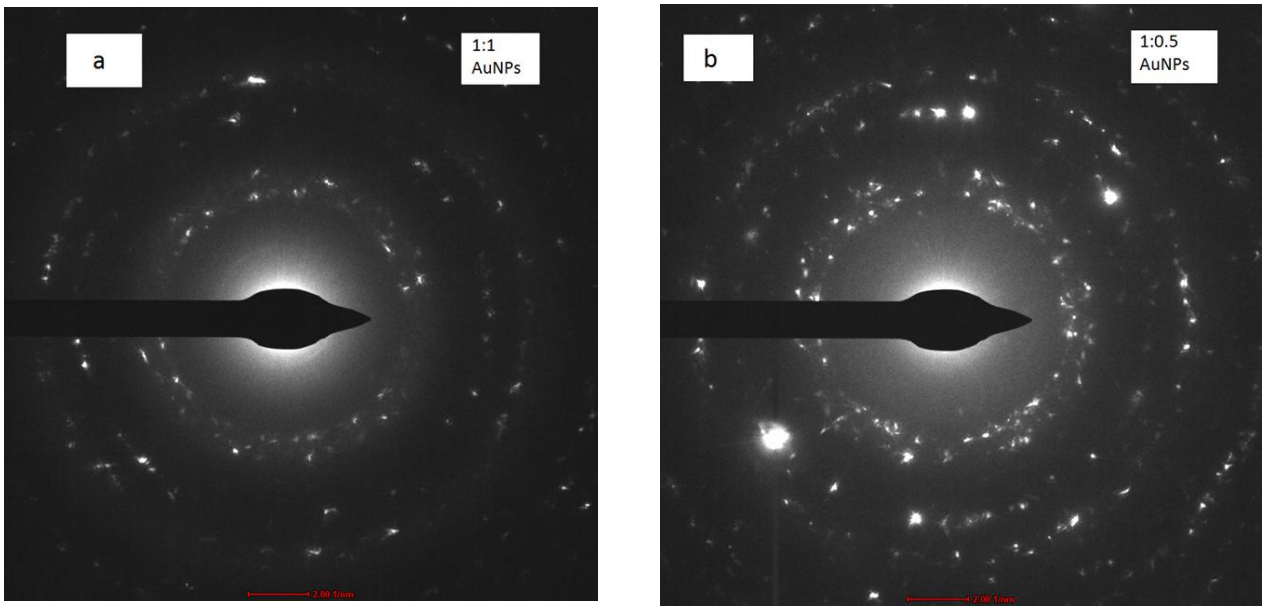

Figure 9. Showing SAED of (a) 1:1 ratio and (b) 1:0.5 ratio.

3.2.2 Degradation of MB

MB has two UV-Vis absorption peaks, one at 664 nm from the MB monomer [46] and one at 612 nm from the MB dimers [47]. Methylene Blue (MB), a heterocyclic dye used in the textile industry, exhibits a characteristic absorption peak at 664 nm resulting from an n-π electronic transition. In its molecular structure, the sulfur and nitrogen atoms link two dimethylamino-substituted aromatic groups. Additionally, two absorption bands are observed in the ultraviolet region (near 245 nm and 290 nm), likely arising from the benzene substituents. In the presence of $NaBH_4$ as a reducing agent, AuNPs significantly accelerated the degradation of MB, acting as heterogeneous catalysts. The dye didn't change color when $NaBH_4$ was added, but gold

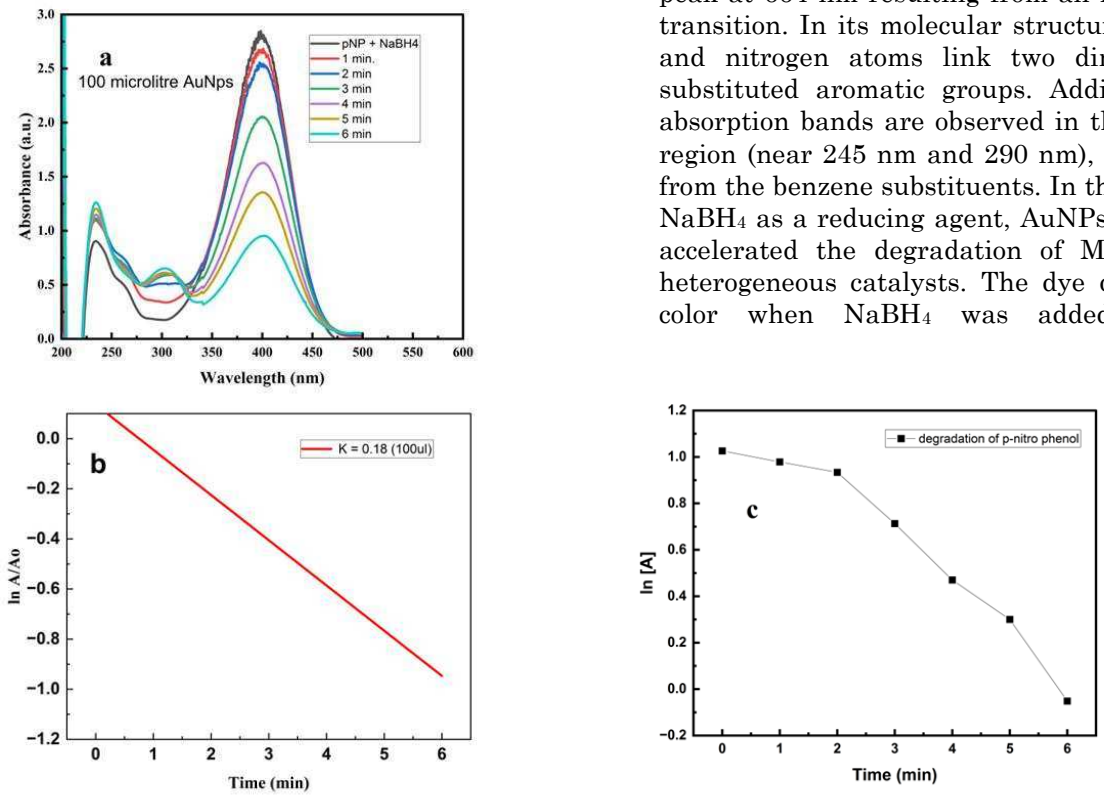

Figure 10. For 50 µL AuNPs Concentration: UV-visible spectra of (a) p-nitro phenol (2 mL, 1×10^{-4} mM) ; consecutive reduction of nitrophenolate ion with time interval of 2 min reacting with $NaBH_4$ (80 µL , 3×10^{-1} M) ; p-amino phenol in presence of Nano catalyst AuNPs (50 µL (b) Plots of ln [*A*/*Ao*] against time for the conversion of p-nitrophenol into p-amino phenol using gold nanoparticles (c) plot of ln [*A*] vs *Time*

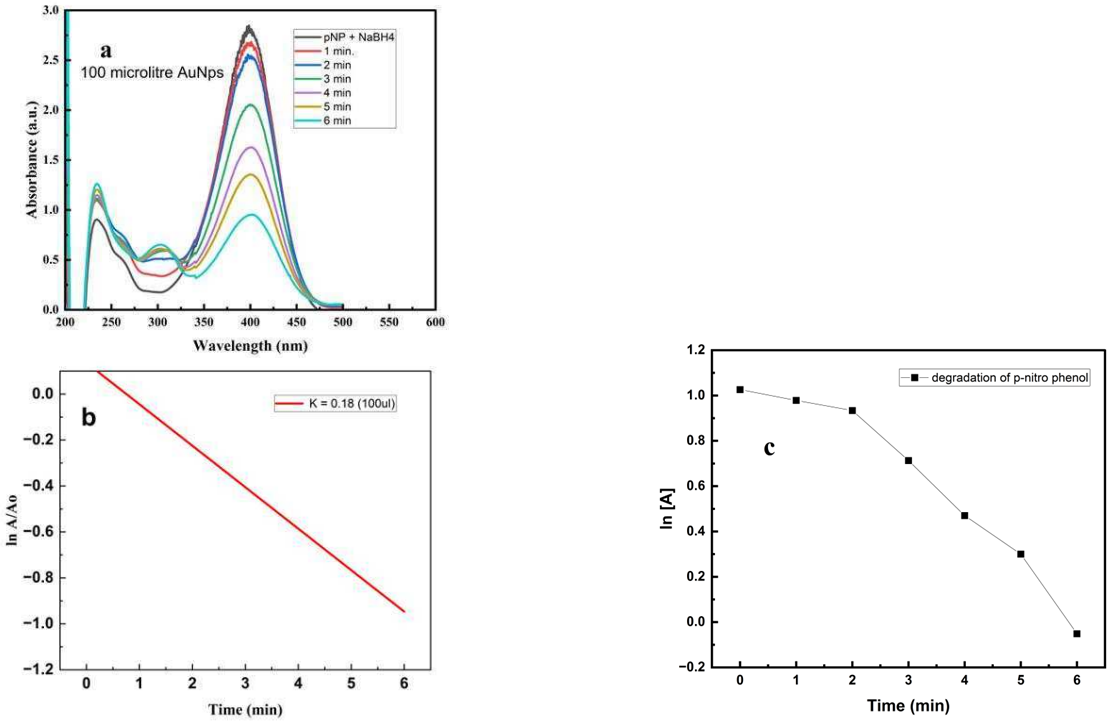

Figure 11. For 100 µL AuNPs Concentration: UV-visible spectra of (a) p-nitro phenol (2 mL, 1×10^{-4} mM); consecutive reduction of nitrophenolate ion with time interval of 2 min reacting with $NaBH_4$ (80 µL , 3×10^{-1} M); p-amino phenol in presence of Nano catalyst AuNPs (100 µL) (b) Plots of ln [A/A_o] against time for the conversion of p-nitrophenol into p-amino phenol using Gold nanoparticles (c) plot of ln [*A*] against time.

nanoparticles decolorized it by forming leuco methylene blue, which is measured by a decrease in absorbance [38]. In the absence of AuNPs, the reaction between MB and $NaBH_4$ resulted in minimal dye degradation. However, when AuNPs were introduced as a catalyst, the degradation of MB was significantly accelerated. The complete degradation of MB occurred within 24 minutes in the absence of AuNPs, while the presence of AuNPs reduced this time to only 5 minutes, as illustrated in Figure 13. This enhanced catalytic activity can be attributed to the large surface area and high reactivity of AuNPs.

The addition of $NaBH_4$ alone did not induce any significant color change in the MB solution. However, upon the addition of AuNPs, the solution gradually decolorized, indicating the formation of Leuco Methylene Blue (LMB), which is characterized by a decrease in absorbance at 665-670 nm, as shown in Figure 13a. This

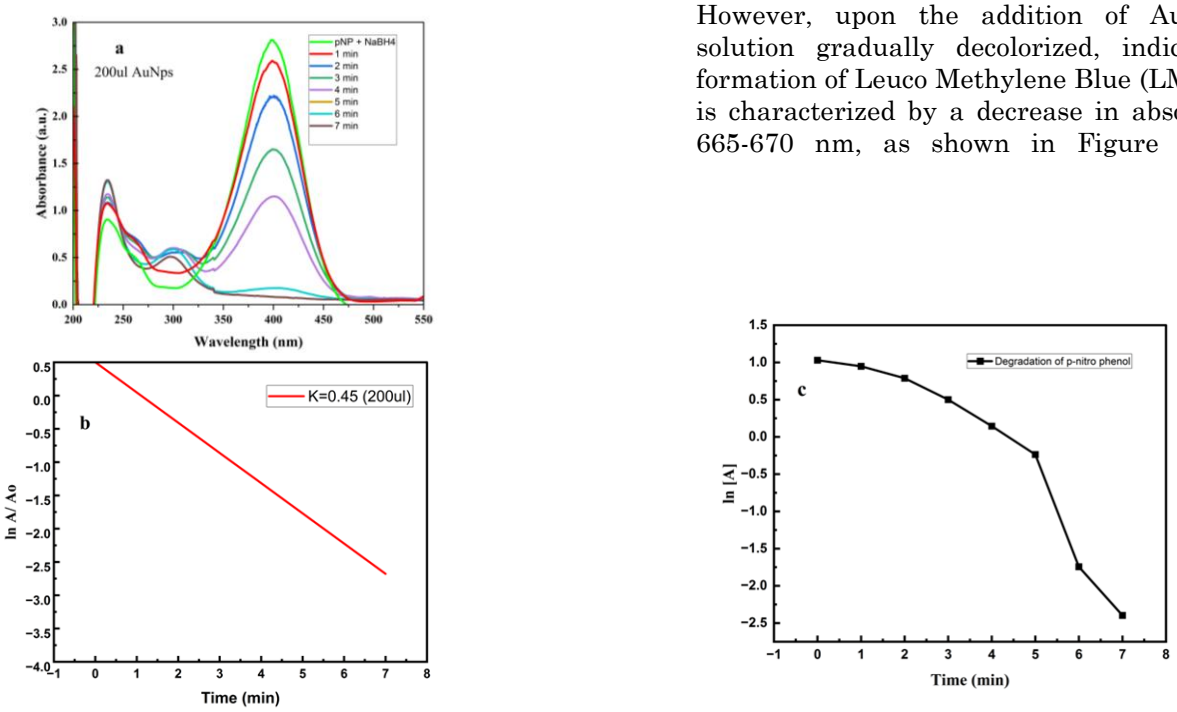

Figure 12. For 200 µl AuNPs Concentration: UV-visible spectra of (a) p-nitro phenol (2 mL,1×10^{-4} mM) ; consecutive reduction of nitrophenolate ion with time interval of 2 min reacting with $NaBH_4$ (80 µL, 3×10^{-1} M); p-amino in presence of Nano catalyst AuNPs (200 µL) (b) Plots of ln [A/A_o] against time for the conversion of p-nitrophenol into p-amino phenol using Gold nanoparticles (c) plot of ln [A] against time.

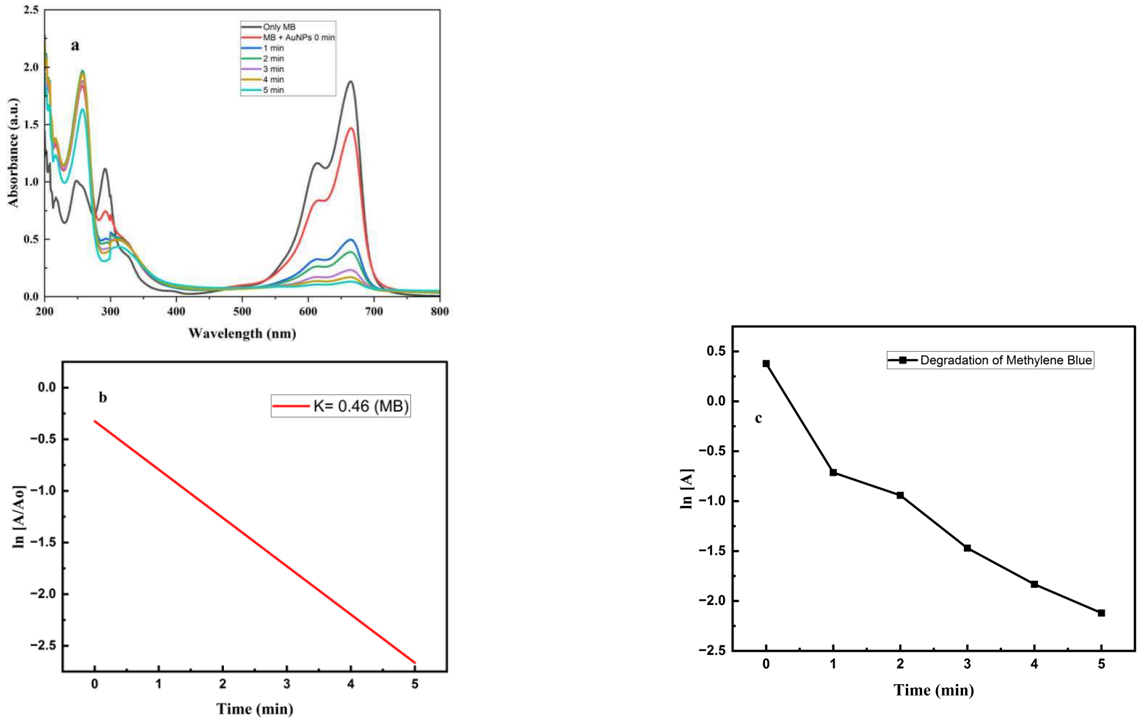

Figure 13. UV-visible spectra of Successive degradation of Methylene blue (1 mL, 1 mM) in 1 mL, 100 mM $NaBH_4$ (a) in presence of nanocatalyst AuNPs (2 mL) (b) Plot of ln [A/A_o] against time (c) Smooth plots of ln [A] against time.

observation confirms that both AuNPs and $NaBH_4$ are essential for the efficient degradation of MB.

Furthermore, AuNPs exhibit a high affinity for both MB and borohydride ions, facilitating their adsorption onto the AuNP surface and promoting the catalytic reaction. The calculated rate constant for the AuNP-catalyzed reaction was 0.46 min^{-1}, further highlighting the significant enhancement in reaction kinetics.

3.2.3 Degradation of MO

Methyl Orange (MO) is an organic azo dye commonly used in the textile and paper industries. Due to its environmental impact, effective methods for its degradation are crucial. One promising approach involves the reduction of MO using $NaBH_4$ in the presence of gold nanoparticles (AuNPs). In this process, MO is adsorbed onto the surface of the AuNPs, facilitating the reduction reaction. As AuNPs are highly reactive and has a large surface area [21], dye molecules and reducing agents bind efficiently to its surface for considerable periods of time, facilitating electron transfer from the borohydride anion to the MO atom. The reaction leads to the formation of an intermediate, which is followed by the oxidation of the azo dye to obtain colorless compounds. The MO dye did not show any change in color when only $NaBH_4$ was added, but when AuNPs were added, the dye became decolored, determined by a decrease in absorbance, and complete degradation was observed after only 7 minutes, as shown in Figure 14a. Rate constant was calculated and it is found to be 0.36 min^{-1}. In the absence of AuNPs, reaction between MO and $NaBH_4$ also occurs, but there is no significant decrease in absorbance. Rate constants of catalytic conversion of p-nitrophenol and dye degradation of MB and MO were found to be same as calculated from formulas and graphs.

The synthesized AuNPs exhibited a high catalytic activity as recorded for the degradation of two water soluble dyes, MB and MO. Degradation efficiency of MB and MO is 91.78% and 91.84% respectively. Kinetic study of the degradation reaction revealed the rates to be pseudo-first order with rate constants 0.46 min^{-1} and 0.36 min^{-1} for MB and MO respectively (Table 2). The rate constant of MB is higher than MO as Methylene blue (MB) exhibits a simpler molecular structure than methyl orange (MO), potentially facilitating its degradation. Additionally, the cationic nature of MB may enhance its adsorption onto the catalytic surface compared to MO. Increased adsorption generally leads to closer proximity of the dye molecules to the active sites of the catalyst, resulting in faster degradation kinetics and a higher rate constant. Schematic representation of catalytic activity of AuNPs are shown in Figure 15. $NaBH_4$ act as electron donor and provides electron to p-nitro phenol, MB and MO.

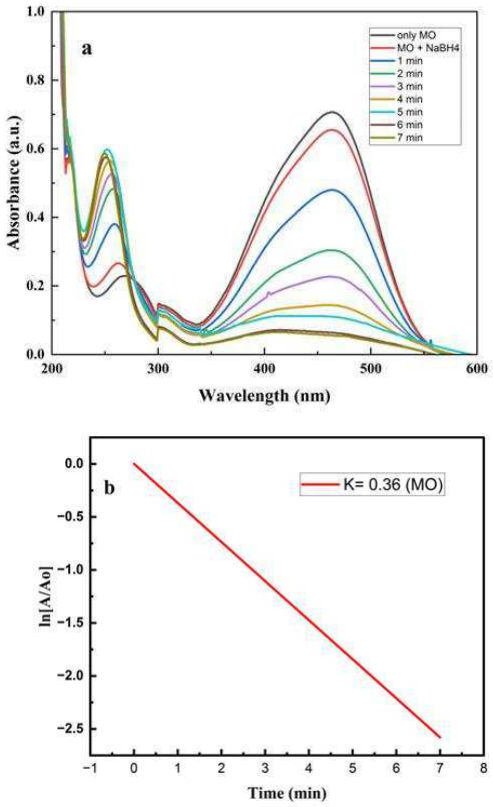

Table 2. Catalytic activity of AuNPs in the degradation of MB and MO.

Dyes	AuNPs concentration	Reaction time (minute)	K (min^{-1})	Correlation Coefficient (R^2)
Methylene Blue	2 mL	5	0.46	1
Methyl Orange	1 mL	7	0.36	0.99

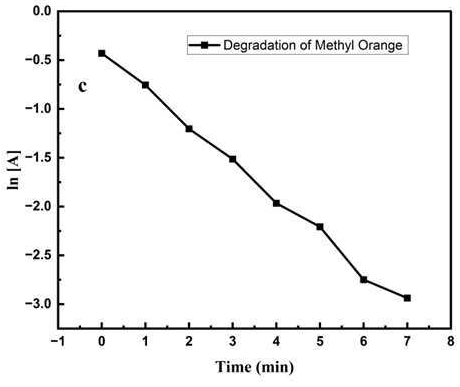

Figure 14. UV -visible spectra of successive degradation of Methylene Orange (50 mL, 10 mg/L) in 2 mL, 0.2 M $NaBH_4$ (a) in presence of nanocatalyst AuNPs (1 mL) (b) Plot of ln [A/A_o] against time (c) Smooth plots of ln [A] against time.

4. Conclusion

In this study, an eco-friendly, simple, and cost-effective one-step synthesis of gold nanoparticles (AuNPs) was successfully achieved using an aqueous extract of Amomum subulatum. The synthesized nanoparticles were characterized, and their catalytic activity was assessed. UV-Visible spectroscopy confirmed the synthesis and stability of the AuNPs over a period of 2 months. TEM and DLS studies revealed that the nanoparticles varied in size and shape. FTIR indicated the predominant presence of 1,8-cineole, which plays a key role in the reduction of chloroauric acid. The synthesized AuNPs exhibited significant catalytic activity in the reduction of p-nitrophenol (4-NP) to p-aminophenol (4-AP) in the presence of $NaBH_4$. Kinetic studies revealed pseudo-first-order reaction kinetics with rate constants increasing with increasing AuNP concentration. The observed catalytic activity can be attributed to the high surface area and ability of AuNPs to lower the activation energy of the reaction. This study also demonstrated the potential of synthesized AuNPs as effective catalysts for the degradation of methylene blue and methyl orange dyes. The environmentally friendly synthesis method, coupled with their observed catalytic efficiency, makes these nanoparticles a promising alternative to those synthesized using conventional chemical methods.

Acknowledgment

The authors thank Sophisticated Analytical Instrument Facility, AIIMS, New Delhi, India for facilitating TEM and DLS measurements.

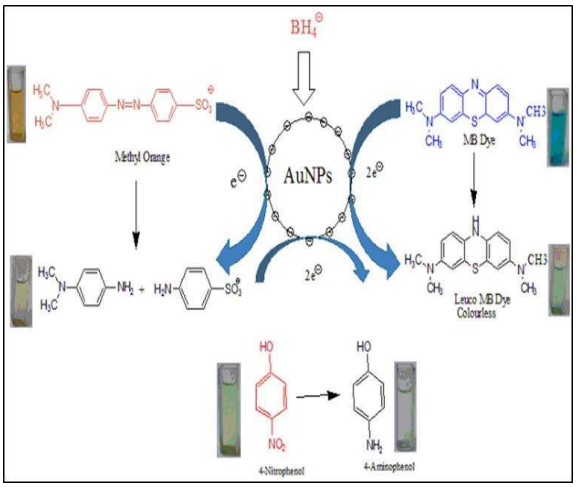

Figure 15. Schematic representation of catalytic activity of AuNPs

CRedit Author Statement

Authors Contributions: Sonam Baghel: performed the experiments and writing the manuscript; Monika Khurana: conceived the original idea, supervision, editing and reviewing. All authors have read and agreed to the published version of the manuscript.

References

[1] Ullah, I., Rauf, A., Khalil, A.A., Luqman, M., Islam, M.R., Hemeg, H.A., Ahmad, Z., Al-Awthan, Y.S., Bahattab, O., Quradha, M.M. (2024). Peganum harmala L. extract-based Gold (Au) and Silver (Ag) nanoparticles (NPs): Green synthesis, characterization, and assessment of antibacterial and antifungal properties. *Food Sci. Nutr.* 1–14. DOI: 10.1002/fsn3.4112

[2] K.M. Sowmya, N.R.T. (2022).Exploring the in-vitro pharmacological characteristics of Gold nanoparticles derived from elettaria cardamomum seed and pod: a comparative study. *Nanotechnol. Reports*. 17, 67–92.

[3] Milanezi, F.G., Meireles, L.M., de Christo Scherer, M.M., de Oliveira, J.P., da Silva, A.R., de Araujo, M.L., Endringer, D.C., Fronza, M., Guimarães, M.C.C., Scherer, R. (2019).Antioxidant, antimicrobial and cytotoxic activities of gold nanoparticles capped with quercetin. *Saudi Pharm. J.* 27, 968–974. DOI: 10.1016/j.jsps.2019.07.005

[4] Muniyappan, N., Pandeeswaran, M., Amalraj, A. (2021). Green synthesis of gold nanoparticles using Curcuma pseudomontana isolated curcumin: Its characterization, antimicrobial, antioxidant and anti- inflammatory activities. *Environ. Chem. Ecotoxicol.* 3, 117–124. DOI: 10.1016/j.enceco.2021.01.002

[5] Dhir, S., Dutt, R., Singh, R.P., Chauhan, M., Virmani, T., Kumar, G., Alhalmi, A., Aleissa, M., Rudayni, H., Al-Zahrani, M. (2023). Amomum subulatum Fruit Extract Mediated Green Synthesis of Silver and Copper Oxide Nanoparticles: Synthesis, Characterization, Antibacterial and Anticancer Activities. *Processes*. 11, 2698. DOI: 10.3390/pr11092698

[6] Nobahar, A., Lourenço, J.P., Costa, M.C., Carlier, J.D. (2024). Printed Circuit Boards Leaching Followed by Synthesis of Gold Nanoparticle Clusters Using Plant Extracts. *Waste and Biomass Valorization*. 15, 1999–2017. DOI: 10.1007/s12649-023-02272-8

[7] Shaabani, E., Amini, S.M., Kharrazi, S., Tajerian, R. (2017). Curcumin coated gold nanoparticles: synthesis, characterization, cytotoxicity, antioxidant activity and its comparison with citrate coated gold nanoparticles. *Nanomed. J.* 4, 115–125. DOI: 10.22038/nmj.2017.21506.1227

[8] Bouttier-Figueroa, D.C., Loreto-Romero, M.A., Roldan, M.A., González-Gutiérrez, F.H., Cortez-Valadez, M., Flores-Acosta, M., Robles-Zepeda, R.E. (2024) Green synthesis of gold nanoparticles via Moringa oleifera seed extract: antioxidant, antibacterial and anticarcinogenic activity on lung cancer. *J. Environ. Sci. Heal. Part A*. 59, 231–240. DOI: 10.1080/10934529.2024.2366736

[9] Donga, S., Bhadu, G.R., Chanda, S. (2020). Antimicrobial, antioxidant and anticancer activities of gold nanoparticles green synthesized using Mangifera indica seed aqueous extract. *Artif. Cells, Nanomedicine Biotechnol.* 48, 1315–1325. DOI: 10.1080/21691401.2020.1843470

[10] Umamaheswari, C., Lakshmanan, A., Nagarajan, N.S. (2018). Green synthesis, characterization and catalytic degradation studies of gold nanoparticles against congo red and methyl orange. *J. Photochem. Photobiol. B Biol.* 178, 33–39. DOI: 10.1016/j.jphotobiol.2017.10.017

[11] Elizarova, T.N., Antopolsky, M.L., Novichikhin, D.O., Skirda, A.M., Orlov, A. V., Bragina, V.A., Nikitin, P.I. (2023). A Straightforward Method for the Development of Positively Charged Gold Nanoparticle-Based Vectors for Effective siRNA Delivery. *Molecules*. 28,. DOI: 10.3390/molecules28083318

[12] Shao, Y., Xu, W., Zheng, Y., Zhu, Z., Xie, J., Wei, X., Zhang, Y., Zhang, J., Wu, Q., Wang, J., Ding, Y. (2023). Interface coordination achieving excellent optical properties of three-dimensional dendritic gold nanoparticles for immunochromatographic performance. *Chem. Eng. J.* 455, 140586. DOI: 10.1016/j.cej.2022.140586

[13] Philip, D. (2010). Green synthesis of gold and silver nanoparticles using Hibiscus rosa sinensis. *Phys. E Low-Dimensional Syst. Nanostructures*. 42, 1417–1424. DOI: 10.1016/j.physe.2009.11.081

[14] Rajan, A., Vilas, V., Philip, D. (2015). Studies on catalytic, antioxidant, antibacterial and anticancer activities of biogenic gold nanoparticles. *J. Mol. Liq.* 212, 331–339. DOI: 10.1016/j.molliq.2015.09.013

[15] Al-Radadi, N.S., Al-Bishri, W.M., Salem, N.A., ElShebiney, S.A. (2024). Plant-mediated green synthesis of gold nanoparticles using an aqueous extract of Passiflora ligularis, optimization, characterizations, and their neuroprotective effect on propionic acid-induced autism in Wistar rats. *Saudi Pharm. J.* 32, 101921. DOI: 10.1016/j.jsps.2023.101921

[16] Shankar, S.S., Rai, A., Ahmad, A., Sastry, M. (2004). Rapid synthesis of Au, Ag, and bimetallic Au core–Ag shell nanoparticles using Neem (Azadirachta indica) leaf broth. *J. Colloid Interface Sci.* 275, 496–502. DOI: 10.1016/j.jcis.2004.03.003

[17] Morrow, G.L. (2022). *Applications of Gold Nanoparticles*. 1st Edition. New York: Nova Science Publisher.

[18] Ismail, M., Xiangke, W., Khan, A.A., Khan, Q. (2023). Amomum subalatum leaf extract derived silver nanoparticles for eco-friendly spectrophotometric detection of Hg (II) ions in water. *Chem. Phys. Impact*. 6, 100148. DOI: 10.1016/j.chphi.2022.100148

[19] Mohammed, A.B.A., Mohamed, A., El-Naggar, N.E.A., Mahrous, H., Nasr, G.M., Abdella, A., Ahmed, R.H., Irmak, S., Elsayed, M.S.A., Selim, S., Elkelish, A., Alkhalifah, D.H.M., Hozzein, W.N., Ali, A.S. (2022). Antioxidant and Antibacterial Activities of Silver Nanoparticles Biosynthesized by Moringa oleifera through Response Surface Methodology. *J. Nanomater.* 2022,. DOI: 10.1155/2022/9984308

[20] Perni, S., Piccirillo, C., Pratten, J., Prokopovich, P., Chrzanowski, W., Parkin, I.P., Wilson, M. (2009). The antimicrobial properties of light-activated polymers containing methylene blue and gold nanoparticles. *Biomaterials*. 30, 89–93. DOI: 10.1016/j.biomaterials.2008.09.020

[21] Shah, A.A., Jayalakshmi, D., Xavier, B. (2021). Characterization of gold nanoparticles synthesized from Solanum torvum (Turkey Berry) fruit extract and its application in catalytic degradation of methylene blue and antibacterial properties. *Mater. Today Proc.* 47, 927–932. DOI: 10.1016/j.matpr.2021.04.606

[22] Sharifi-Rad, M., Pohl, P., Epifano, F., Álvarez-Suarez, J.M. (2020). Green synthesis of silver nanoparticles using astragalus tribuloides delile. Root extract: Characterization, antioxidant, antibacterial, and anti-inflammatory activities. *Nanomaterials*. 10, 1–17. DOI: 10.3390/nano10122383

[23] Alduraihem, N.S., Bhat, R.S., Al-Zahrani, S.A., Elnagar, D.M., Alobaid, H.M., Daghestani, M.H. (2023). Anticancer and Antimicrobial Activity of Silver Nanoparticles Synthesized from Pods of Acacia nilotica. *Processes*. 11, 1–16. DOI: 10.3390/pr11020301

[24] Koryagin, A.S., Mochalova, A.E., Salomatina, E. V., Eshkova, O.Y., Smirnova, L.A. (2013). Adaptogenic effects of chitosan-gold nanocomposites under simulated hypoxic conditions. *Inorg. Mater. Appl. Res.* 4, 127–130. DOI: 10.1134/S2075113313020081

[25] Aftab, R. A., Zaidi, S., Danish, M., Danish, M., Ansari, K. B., Rao, R. A. K., & Qyyum, M.A. (2023). Herbal medicinal waste black cardamom (Amomum subulatum) as a novel adsorbent for removing Cd(II) from water. *Int. J. Environ. Sci. Technol.* 1–20. DOI: 10.1007/s13762-023-04996-5

[26] Ahmad Aftab, R., Zaidi, S., Aslam Parwaz Khan, A., Arish Usman, M., Khan, A.Y., Tariq Saeed Chani, M., Asiri, A.M. (2023). Removal of congo red from water by adsorption onto activated carbon derived from waste black cardamom peels and machine learning modeling. *Alexandria Eng. J.* 71, 355–369. DOI: 10.1016/j.aej.2023.03.055

[27] Shabestarian, H., Homayouni-Tabrizi, M., Soltani, M., Namvar, F., Azizi, S., Mohamad, R., Shabestarian, H. (2017). Green synthesis of gold nanoparticles using sumac aqueous extract and their antioxidant activity. *Mater. Res.* 20, 264–270. DOI: 10.1590/1980-5373-MR-2015-0694

[28] Singh, A.K., Tripathi, M., Srivastava, O.N., Verma, R.K. (2017). Silver Nanoparticles/Gelatin Composite: A New Class of Antibacterial Material. *ChemistrySelect*. 2, 7233–7238. DOI: 10.1002/slct.201701245

[29] Sharada S, O. V. (2015). Green Synthesis and Characterization of Silver Nanoparticles and Evaluation of their Antibacterial Activity using Elettaria Cardamom Seeds. *J. Nanomed. Nanotechnol.* 06, 2–5. DOI: 10.4172/2157-7439.1000266

[30] Singh, A.K., Srivastava, O.N. (2015). One-Step Green Synthesis of Gold Nanoparticles Using Black Cardamom and Effect of pH on Its Synthesis. *Nanoscale Res. Lett.* 10, 1–12. DOI: 10.1186/s11671-015-1055-4

[31] Noah, N. (2019). Green synthesis: Characterization and application of silver and gold nanoparticles. In: *Green Synthesis, Characterization and Applications of Nanoparticles*. pp. 111–135. Elsevier (2019)

[32] Wang, J., Li, Y., Lu, Q., Hu, Q., Liu, P., Yang, Y., Li, G., Xie, H., Tang, H. (2021). Drying temperature affects essential oil yield and composition of black cardamom (Amomum tsao-ko). *Ind. Crops Prod.* 168,. DOI: 10.1016/j.indcrop.2021.113580

[33] Küp, F.Ö., Çoşkunçay, S., Duman, F. (2020). Biosynthesis of silver nanoparticles using leaf extract of Aesculus hippocastanum (horse chestnut): Evaluation of their antibacterial, antioxidant and drug release system activities. *Mater. Sci. Eng. C*. 107, 110207. DOI: 10.1016/j.msec.2019.110207

[34] Dauthal, P., Mukhopadhyay, M. (2012). Prunus domestica fruit extract-mediated synthesis of gold nanoparticles and its catalytic activity for 4-nitrophenol reduction. *Ind. Eng. Chem. Res.* 51, 13014–13020. DOI: 10.1021/ie300369g

[35] Das, J., Velusamy, P. (2014). Catalytic reduction of methylene blue using biogenic gold nanoparticles from Sesbania grandiflora L. *J. Taiwan Inst. Chem. Eng.* 45, 2280–2285. DOI: 10.1016/j.jtice.2014.04.005

[36] Edison, T.J.I., Sethuraman, M.G. (2012). Instant green synthesis of silver nanoparticles using Terminalia chebula fruit extract and evaluation of their catalytic activity on reduction of methylene blue. *Process Biochem.* 47, 1351–1357. DOI: 10.1016/j.procbio.2012.04.025

[37] Singh, I., Gupta, S., Gautam, H.K., Dhawan, G., Kumar, P. (2021). Antimicrobial, radical scavenging, and dye degradation potential of nontoxic biogenic silver nanoparticles using Cassia fistula pods. *Chem. Pap.* 75, 979–991. DOI: 10.1007/s11696-020-01355-3

[38] Joseph, S., Mathew, B. (2015). Microwave-assisted green synthesis of silver nanoparticles and the study on catalytic activity in the degradation of dyes. *J. Mol. Liq.* 204, 184–191. DOI: 10.1016/j.molliq.2015.01.027

[39] Moores, A., Goettmann, F.: (2006).The plasmon band in noble metal nanoparticles: an introduction to theory and applications. *New J. Chem*. 30, 1121–1132. DOI: 10.1039/B604038C

[40] Boruah, J.S., Devi, C., Hazarika, U., Bhaskar Reddy, P.V., Chowdhury, D., Barthakur, M., Kalita, P. (2021). Green synthesis of gold nanoparticles using an antiepileptic plant extract: in vitro biological and photo-catalytic activities. *RSC Adv.* 11, 28029–28041. DOI: 10.1039/D1RA02669K

[41] Jalab, J., Abdelwahed, W., Kitaz, A., Al-Kayali, R. (2021). Green synthesis of silver nanoparticles using aqueous extract of Acacia cyanophylla and its antibacterial activity. *Heliyon*. 7, e08033. DOI: 10.1016/j.heliyon.2021.e08033

[42] Rezazadeh, N.H., Buazar, F., Matroodi, S. (2020). Synergistic effects of combinatorial chitosan and polyphenol biomolecules on enhanced antibacterial activity of biofunctionalaized silver nanoparticles. *Sci. Rep.* 10, 1–13. DOI: 10.1038/s41598-020-76726-7

[43] Danaei, M., Dehghankhold, M., Ataei, S., Hasanzadeh Davarani, F., Javanmard, R., Dokhani, A., Khorasani, S., Mozafari, M.R. (2018). Impact of particle size and polydispersity index on the clinical applications of lipidic nanocarrier systems. *Pharmaceutics*. 10, 1–17. DOI: 10.3390/pharmaceutics10020057

[44] Ebnesajjad, S. (2010). *Handbook of adhesives and surface preparation*. 1st Edition. William Andrew Publishing.

[45] Mishra, A.K., Tiwari, K.N., Saini, R., Kumar, P., Mishra, S.K., Yadav, V.B., Nath, G. (2020). Green Synthesis of Silver Nanoparticles from Leaf Extract of Nyctanthes arbor-tristis L. and Assessment of Its Antioxidant, Antimicrobial Response. *J. Inorg. Organomet. Polym. Mater.* 30, 2266–2278. DOI: 10.1007/s10904-019-01392-w

[46] Rauf, M.A., Meetani, M.A., Khaleel, A., Ahmed, A. (2010). Photocatalytic degradation of Methylene Blue using a mixed catalyst and product analysis by LC/MS. *Chem. Eng. J.* 157, 373–378. DOI: 10.1016/j.cej.2009.11.017

[47] Flores, N.M., Pal, U., Galeazzi, R., Sandoval, A. (2014). Effects of morphology{,} surface area{,} and defect content on the photocatalytic dye degradation performance of ZnO nanostructures. *RSC Adv.* 4, 41099–41110. DOI: 10.1039/C4RA04522J